Photochemical Reaction Dynamics of $O(^1D)$ with Saturated Hydrocarbons, CH_4, C_2H_6, and C_3H_8, under Bulk Conditions and in van der Waals Complexes

Shin-ichi Wada[†] **and Kinichi Obi***[,‡]

Department of Chemistry, Tokyo Institute of Technology, Ohokayama, Meguro, Tokyo 152-8551, Japan

Received: October 15, 1997; In Final Form: January 13, 1998

The reactions of $O(^1D)$ atom with saturated hydrocarbons (RH), CH_4, C_2H_6, and C_3H_8, were studied by monitoring the laser induced fluorescence of products OH in the $v'' = 0$ and 1 levels under bulk conditions and in van der Waals complexes, $N_2O{\cdot}RH$. $O(^1D)$ was produced by the ArF excimer laser photolysis of N_2O. Nascent rotational distributions are bimodal in all cases; the low- and high-*N* components. The former is formed from a long-lived collision complex generated by the insertion process. The collision complex has enough lifetime to randomize excess energy before decomposition. The high-*N* component is produced in the short-lived insertion process, in which the collision energy of $O(^1D)$ atoms is reflected in the rotational energy. The spin−orbit state in the only half-reactions producing the $v'' = 0$ level shows large population in the low-lying $^2\Pi_{3/2}$ state in low-*N* components, though spin−orbit populations are statistical in other reaction systems studied. The reaction proceeds via a transfer from a singlet reaction surface to a triplet surface keeping the conservation of the electronic angular momentum.

1. Introduction

The electronically excited oxygen atom, $O(^1D)$, is highly reactive with various molecules and causes both abstraction and insertion reactions in different from the ground state, $O(^3P)$.[1−3] The reactions with simple saturated hydrocarbons, especially methane, are important in upper atmospheric chemistry[3,4] and generate the OH radical, which is an important intermediate of the catalytic HO_x cycle in the lower stratosphere because the HO_x cycle is one of the mechanisms most responsible for O_3 destruction.[5]

The reaction of $O(^1D)$ with hydrocarbons is known to proceed without a barrier, and the cross-section is large, nearly the gas kinetic limit. Since the first study was reported by Basco and Norrish,[6] the $O(^1D)$ + hydrocarbon reaction systems have been widely studied by several groups.[7−22] The early studies supported that the main products were OH and alkyl radicals, which were formed through two parallel mechanisms. The dominant reaction mechanism is insertion of an $O(^1D)$ atom into the C−H bond, resulting in chemically activated alcohol followed by fragmentation. This reaction mechanism was confirmed by the detection of stable alcohol under the high-pressure condition, in which chemically activated intermediate, $[ROH]^\dagger$, was collisionally stabilized before dissociation. However, OH radicals were also observed under the high-pressure condition. The formation of OH radicals was ascribed to the direct abstraction of H atom by $O(^1D)$ atom, not via the activated intermediate.

Although OH and alkyl radicals are main products in these reactions, other paths were also reported. One is the weaker C−C bond cleavage of the chemically activated alcohol. This reaction path is more dominant in the reaction with larger hydrocarbons. The formation of molecular hydrogen from the intermediate was also reported.[8,9] Hydrogen atom generation was shown in a crossed molecular beam experiment for the reaction of $O(^1D)$ with CH_4, and the molecular hydrogen elimination was estimated to be less than 25% of the atomic elimination.[10]

Recent studies about nascent internal distributions of products[13−20] and ab initio calculations[21,22] for the reaction of $O(^1D)$ with simple saturated hydrocarbons producing OH and alkyl radicals throw light on its reaction dynamics. Luntz reported that rotational distribution of OH was characterized by bimodal modes for all reactants; the rotationally and vibrationally hot and cold $OH(X\ ^2\Pi)$.[13] The former is dominant for CH_4 and produced by the dissociation of the short-lived intermediate prior to energy equilibration, where the reaction mechanism is similar to the reaction of $O(^1D)$ with H_2. The latter product is considered to be generated by the abstraction reaction because of the similar distribution to that in the reaction of $O(^3P)$ with hydrocarbon.[23] This mechanism is more dominant for larger hydrocarbons. On the other hand, Park and Wiesenfeld reported on the basis of more complete measurements of the product OH that the rotationally and vibrationally cold OH might be ascribed to the insertion mechanism forming long-lived intermediate alcohol, in which excess energy was sufficiently randomized among vibrations prior to fragmentation.[17]

Naaman and co-workers made the crossed molecular beam experiments of the reaction of $O(^1D)$ with monomers and clusters of simple saturated hydrocarbons, and observed the propensities for populating the lower lying spin−orbit F_1 component in lower rotational levels only in the CH_4 cluster and C_3H_8 monomer reactions.[18] Recently, the OH distributions in the reaction of $O(^1D)$ with CH_4 was studied using $O_3{\cdot}CH_4$ van der Waals (vdW) complex by van Zee et al.[20a] It was found that the populations were essentially identical to those reported by Naaman and co-workers except for slight difference in the rotational distribution for $v'' = 0$. They also tried to reveal the reaction mechanism by measuring the rise rate of OH products with the subpicosecond pump−probe technique and observed only one component with 3 ps rise time.[20b] Therefore, two mechanisms could not be well distinguished.

In this study, reactions of $O(^1D)$ atom with simple saturated hydrocarbons, CH_4, C_2H_6, and C_3H_8, are studied under bulk

[†] Present address: Department of Physical Science, Hiroshima University, Higashi-Hiroshima 739-8526, Japan.

[‡] Present address: Department of Chemical and Biological Sciences, Japan Women's University, Mejirodai, Bunkyoku, Tokyo 112-8681, Japan

S1089-5639(97)03344-6 CCC: $15.00
Published on Web 04/23/1998

condition and in vdW complex to obtain further understanding of the reaction dynamics. The reactions were investigated by monitoring the product OH with the laser-induced fluorescence (LIF) method. $O(^1D)$ atom was generated by the 193 nm photodissociation of N_2O,

$$N_2O + h\nu(193\ \text{nm}) \rightarrow O(^1D) + N_2(X^1\Sigma_g^+) \quad (1)$$

and reacted with hydrocarbons in the bulk reaction

$$O(^1D) + RH \rightarrow OH(X\ ^2\Pi) + R\cdot \quad (2)$$

and in the half-reaction

$$N_2O\cdot RH + h\nu(193\ \text{nm}) \rightarrow OH(X\ ^2\Pi) + R\cdot + N_2 \quad (3)$$

$$R\cdot = CH_3, C_2H_5, C_3H_7$$

The purpose of this paper is to verify the mechanism forming OH product and investigate its characteristics. The average translational energy of $O(^1D)$ atom produced here is higher than those in the photolysis of O_3 studied before. Due to the large reaction exothermicity, the available energy is not significantly varied by changing the experimental conditions: for example, in the $O(^1D) + CH_4$ reactions photoinitiated by the 193 nm photolysis of N_2O and 248 nm of O_3, the average collision energies are 38.9 and 26.7 kJ mol^{-1}, while the available energies are 222 and 210 kJ mol^{-1}, respectively. It is expected that the collision energy is reflected in the internal energy distribution of the reaction products. It is, therefore, possible to understand how collision energy influences the reaction dynamics in such a reaction system with large reaction exothermicity.

2. Experimental Section

Experiments were carried out by using the laser photolysis/LIF pump−probe technique in a flow cell and a supersonic jet. The reaction between $O(^1D)$ and saturated hydrocarbons was initiated by irradiation of photolysis laser to mixtures or vdW complex of N_2O and saturated hydrocarbons, and the population of the specific quantum states of the reaction product, OH($X\ ^2\Pi\ v'', N'', \Omega'', \Lambda''$) was measured with the LIF method.

Bulk Experiments. Samples (N_2O and saturated hydrocarbon) which were premixed in a stainless steel cylinder were flowed into a stainless steel cell and pumped away by a rotary pump (Alcatel M2021C, 275 L/min) equipped with a mechanical booster pump (Ulvac PMB-001B, 1500 L/min). Total pressure was controlled by a needle valve and monitored by a capacitance manometer (MKS Baratron, 227HS-1). Partial pressures were maintained at 19 mTorr for N_2O and 61 mTorr for hydrocarbon. An ArF excimer laser (Lambda Physik COMPex 102) was focused with a 500 mm focal length lens into the cell and photolyzed N_2O to generate $O(^1D)$ atom. Output of a dye laser (Lambda Physik FL 2002, sulforhodamine B and rhodamine 101 dyes) pumped by a XeCl excimer laser (Lambda Physik COMPex 102) was frequency-doubled with a KDP crystal and irradiated to detect the 0−0 and 1−1 sequence bands of the OH $A\ ^2\Sigma^+ - X\ ^2\Pi$ transition. The two laser beams were counter-propagated collinearly. The lasers were operated at 10 Hz, where samples were enough to be refreshed shot by shot. The delay time between the photolysis and probe lasers was kept as short as possible to minimize collisional quenching and at 100 ns in the experiments.

The fluorescence signals were collected with a lens system located at a right angle to the laser beams and focused onto a photomultiplier tube (Hamamatsu R212UH) through cutoff (Toshiba 9−54) and band-path (Hoya U340) filters. The output signals amplified by a preamplifier (Stanford SR-240) were integrated with a gated integrator (Stanford SR-250), digitized with an A/D converter (Stanford SR-245), and transferred to a personal computer. Laser intensities were monitored with photodiodes (Hamamatsu S1336−5BQ) for the photolysis and probe lasers and integrated simultaneously.

The measured population is disturbed by rotational relaxation in the $A\ ^2\Sigma^+$ state by collisions. It was estimated that the population was affected at most 14% under our experimental condition, which was within experimental error and no correction was made.

Jet Experiments. Premixed gas was expanded through a pulsed solenoid nozzle (General Valve, P/N 9-279-900), which was equipped with a conical chip ($\Phi = 300\ \mu$m) at the nozzle exit to form vdW complexes efficiently. The ratio of samples was typically 2% N_2O, 4% hydrocarbon, and 94% Ar. As large clusters, such as $(N_2O)_n\cdot(RH)_m$, would be formed at high stagnation pressure, typical sample gas pressure was kept at 2 atm to form $N_2O\cdot RH$. A chamber was evacuated with a 6 in. oil diffusion pump (Ulvac ULK-06, 1400 L/s) with a water baffle and a mechanical rotary pump (Ulvac D-950, 960 L/min). The pressure in the chamber was kept at several degree of 10^{-5} Torr during the nozzle operation to prevent bulk reaction within the jet.

$N_2O\cdot RH$ vdW complex was photolyzed by the ArF laser at X/D = 40−60 to prepare $O(^1D)$−RH reactant pairs. The probe laser was counter-propagated collinearly, and the laser beams, molecular beam, and detection system were mutually orthogonal. The fluorescence signals were collected by the same manner mentioned above.

Under the jet condition, a strong emission was observed just after the irradiation of the ArF excimer laser. To avoid the influence of the emission, the probe laser was fired at 200 ns after the photolysis laser, and if necessary an interference band-path filter (Corion G10−307) was also used. Spectra of OH were corrected for the transmission profile of the interference filter due to its narrow half-width (10 nm fwhm centered at 308.8 nm).

Hydrocarbons used in this experiment do not absorb 193 nm light.[24] However, there is the possibility that H atom is generated by the 193 nm multiphoton absorption of hydrocarbon and reacts with N_2O producing OH. Actually chemiluminescence due to the 193 nm multiphoton absorption of hydrocarbon appeared by the irradiation of ArF excimer laser. To examine the influence of H atom, the OH LIF signal intensity was measured by changing the 193 nm laser power. The results give linear relations for three hydrocarbons. This confirms that the OH radical is produced by the reaction of $O(^1D)$ with hydrocarbons following the absorption of a single 193 nm photon and that the H atom does not affect the LIF signal intensity of OH.

Nascent Population. The saturation of the OH LIF intensity would occur due to the large probability of the $A\ ^2\Sigma^+ - X\ ^2\Pi$ transition. The signal intensity was confirmed to be linear against the probe laser power up to 6 μJ/pulse. The output of the probe laser was therefore attenuated through an appropriate neutral density filter and kept at ~3 μJ/pulse to prevent the saturation of the OH signals. Figure 1 shows the LIF excitation spectra for (a) the bulk and (b) half-reactions of $O(^1D)$ with CH_4. The spectra were calibrated for the intensities of photolysis and probe lasers. Rotational band assignments were carried out after the table of Dieke and Crosswhite.[25] The nascent population of each rovibrational state was determined from the measured LIF signal intensity by using the reported

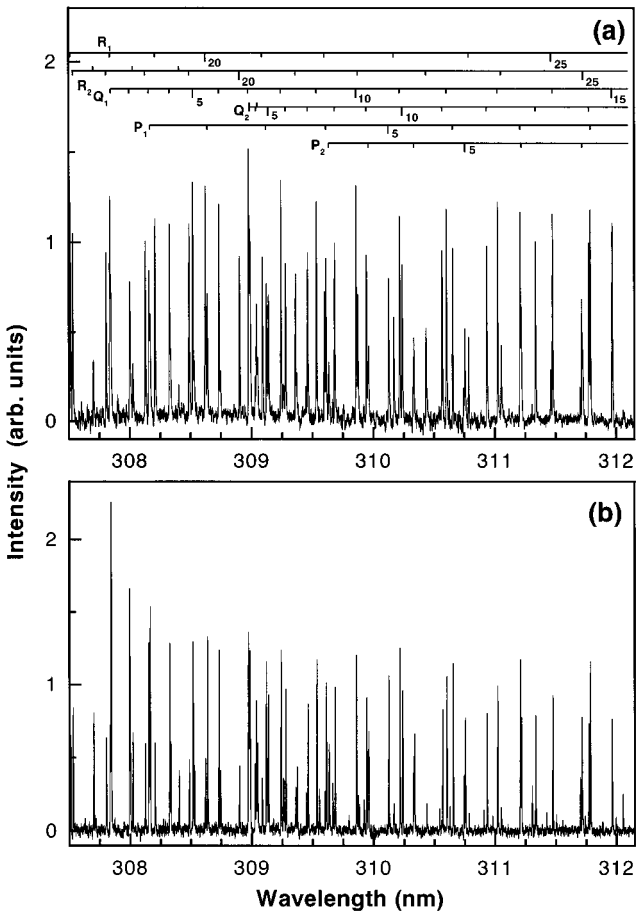

Figure 1. LIF excitation spectra in the 0−0 band regions of nascent OH produced in the CH_4 (a) bulk and (b) half-reactions. Assignments are indicated in (a). Experimental conditions are described in the text.

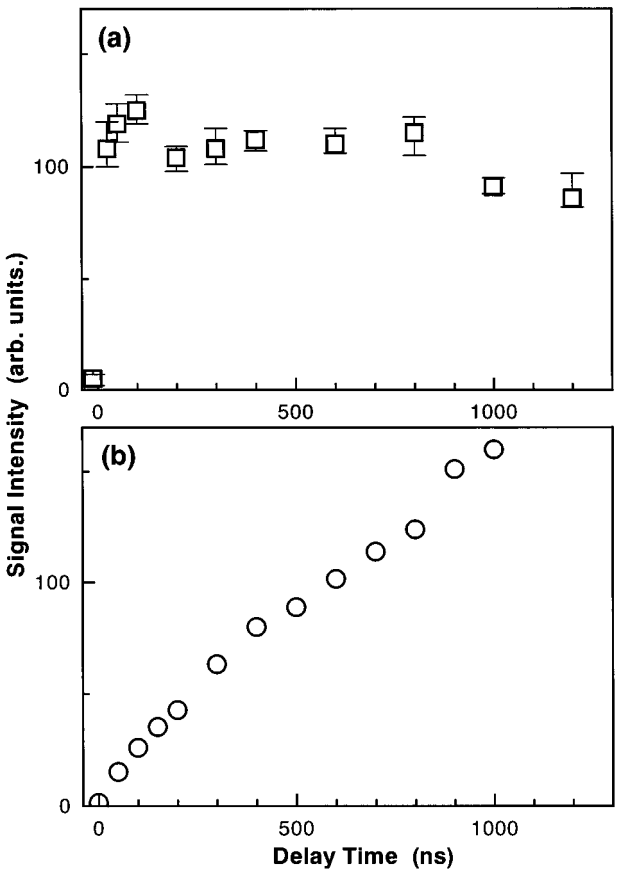

Figure 2. LIF signal intensities of product OH as a function of the delay time between photolysis and probe lasers in the C_2H_6 reaction under the jet condition (a) and the CH_4 bulk reaction (b). The signals were measured at the $Q_1(1)$ line in the OH A $^2\Sigma^+ - X^2\Pi$ transition.

Einstein *B* coefficient[26] and the fluorescence lifetime[27] of the rovibrational levels in the A $^2\Sigma^+$ state. The *P*, *Q*, and *R* main branches are usually used to analyze the LIF signal intensity. However, the satellite lines are also used when main and satellite lines overlap (in the low-*N* region) or main line does not exist ($P_2(1)$). Since both $v' = 0$ and 1, OH(A $^2\Sigma^+$) predissociate in higher rotational levels, the fluorescence quantum yield of the rovibrational levels was taken into accounts to determine the nascent rotational distribution for $N' \geq 25$ and 16 for $v' = 0$ and 1, respectively.

Inspection of Reactant Precursor in the Jet. When N_2O was photolyzed at 193 nm, O(1D) is produced with large translational energy compared with the case of O_3. As the average translational energy of O(1D) is 114 kJ mol^{-1} in the photodissociation of N_2O,[28] the average relative velocity of O(1D) in the N_2O/RH complex is estimated to be ∼3.0 km s^{-1} in the center of mass system. Since O atom travels several 10 μm in the ns order detection time scale at this velocity, we should examine the possibility of bulk reaction as well as the collisional relaxation of product OH in the jet.

Figure 2 shows the LIF signal intensities as a function of the delay time between the photolysis and probe lasers under (a) the jet and (b) bulk conditions. LIF signal was measured by using the $Q_1(1)$ line in the OH A $^2\Sigma^+ - X^2\Pi$ transition. The intensity under the bulk condition increases monotonically with increase in the delay time. This rise is mainly due to increase of collision number between O(1D) and hydrocarbon, which results in increase of OH production as time passes. On the other hand, the signal intensity under the jet condition is almost constant from the very short delay time. If the bulk reaction would occur and produce OH radical in the jet, LIF signal intensity ought to increase with time. Actually, such a slow rise was observed even in the jet when He gas was used as a carrier gas instead of Ar or X/D was small. Therefore, the half-reaction was carried out with Ar carrier gas and at sufficient large value of X/D. The constant intensity of LIF signals on delay time seen in Figure 2a is a reliable evidence that the reaction occurs in a vdW complex. Decrease of the LIF signal in the later time region after 1μs is mainly due to the escape of product OH from the detection region in the jet.

The rotational relaxation would also result in the slow rise of LIF signal, if it occurs. The effect of rotational relaxation is, however, ignored from the result shown in Figure 2a. This is also confirmed from the same measurements done by using the $R_1(20)$ line for the higher rotational level, which showed no dependence of LIF intensity on delay time.

Naaman and co-workers reported drastic cooling of OH rotation in the crossed molecular beam reaction of O(1D) with the CH_4 cluster.[18] Preliminary experiments were, thus, done to examine the formation of OH from large clusters, $(N_2O)_n \cdot (RH)_m$. The LIF signal intensities were measured by changing concentration of N_2O or hydrocarbon of premixed gas. Concentrations were changed up to 10%. The results showed almost linear dependence for both gases. It is concluded that OH was produced in the reaction of 1:1 vdW complex, $N_2O \cdot RH$.

Chemicals. Chemicals, N_2O (Shouwa Denko, 99%), CH_4 (Takachiho 99%), C_2H_6 (Takachiho 99.7%), C_3H_8 (Takachiho 99.9%), and Ar (Takachiho 99.9999%) were used without further purification.

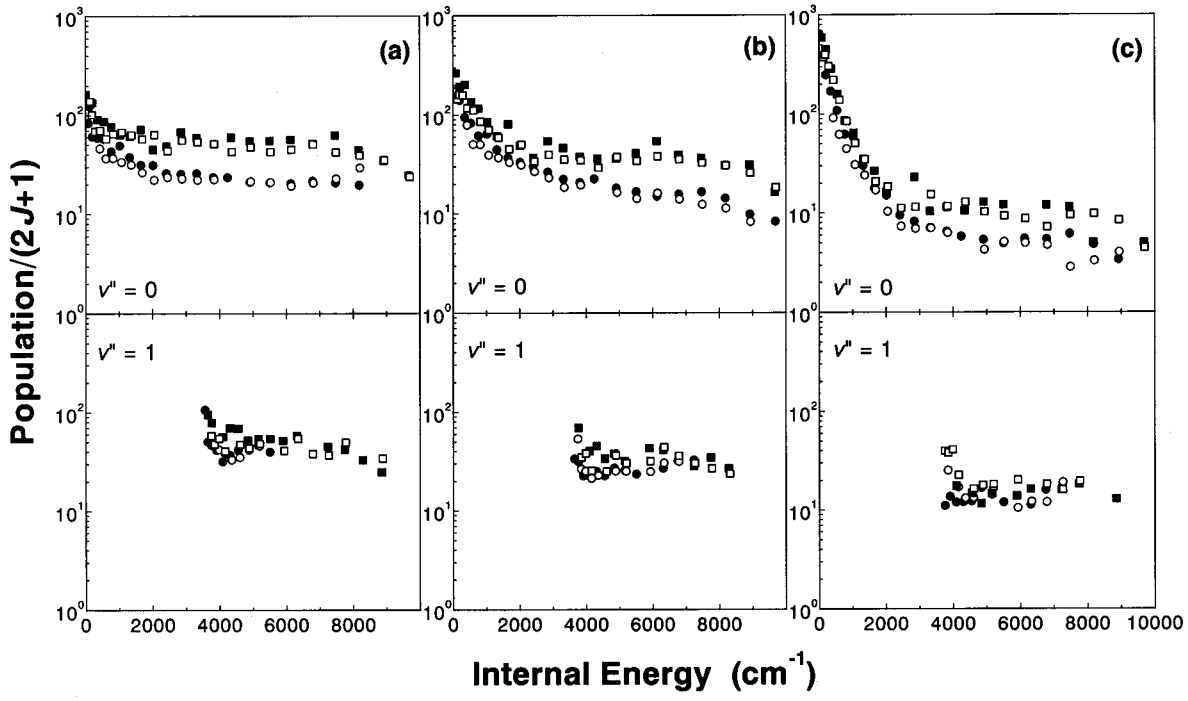

Figure 3. Nascent rotational distributions for $v'' = 0$ (upper) and 1 (lower) levels of product OH($X\ ^2\Pi$) produced in the bulk reactions of $O(^1D)$ with (a) CH_4, (b) C_2H_6, and (c) C_3H_8. Symbols: ■, $F_1\Pi(A')$; □, $F_2\Pi(A')$; ●, $F_1\Pi(A'')$; and ○, $F_2\Pi(A'')$.

3. Results

A. Reactions under Bulk Collision Conditions. *Rotational Population.* As discussed in Experimental Section, the LIF excitation spectra of product OH measured under the bulk conditions reflect nascent populations of $OH(X^2\Pi)$. The nascent rotational distributions obtained are shown in Figure 3 for $v'' = 0$ (upper) and 1 (lower) of the OH ($X\ ^2\Pi$) product in the bulk reaction of $O(^1D)$ with (a) CH_4, (b) C_2H_6, and (c) C_3H_8. The distributions in Figure 3 are described by logalismic plots of populations divided by the rotational degeneracy, $2J'' + 1$, as a function of internal rotational energy like a Boltzmann plot. Highly rotational excitation was observed in all reactions; up to $N'' = 26$ for $v'' = 0$ and $N'' = 18$ for $v'' = 1$. The rotational distribution in $O(^1D) + C_3H_8$ reaction shows much richer population in low-N region than that in $O(^1D) + CH_4$. Park and Wiesenfeld reported that the rotational distribution in the reaction of $O(^1D)$ with CH_4 initiated by the 248 nm photolysis of O_3 was characterized by an essentially unimodal mode, while the C_3H_8 reaction apparently gave a bimodal distribution.[17] The one component has population on only lower rotational levels (low-N component), and the other has broad population lasting to higher levels (high-N component). The present results shows the similar distributions to the reported ones which show obviously the bimodal distribution in $v'' = 0$ levels for all reactant hydrocarbons. In the CH_4 reaction the rotational distribution is mainly governed by the high-N component with slight contribution of the low-N one, while the low-N component becomes more dominant for the larger hydrocarbons. The distributions in the $v'' = 1$ level are bimodal and similar in all reactions.

The first study of OH nascent distribution was done by using 266 nm O_3 photolysis as an $O(^1D)$ source.[13] It was reported that all distributions were bimodal and that the high-N component was predominantly formed for small hydrocarbons (CH_4, C_2H_6) and the low-N component for large ones (C_3H_8, $C(CH_3)_4$). The former was attributed to the insertion/elimination reaction, and the latter was to the direct abstraction. Lately, Park and Wiesenfeld,[17] who photoinitiated the reactions by the 248 nm photolysis of O_3, reported that both bimodal components were produced through the insertion/elimination mechanism. The high-N component arose from prompt dissociation of a collision complex before energy released by the reaction was statistically distributed among the internal modes and the low-N from dissociation of a long-lived complex after the randomization of internal energy instead of the direct abstraction. The present results obtained in the reactions initiated by the 193 nm photolysis of N_2O show similar distributions to the reported ones. However, the high-N component is more populated for all reactants comparing with those reported by Park and Wiesenfeld. The populations in the low-N components for C_2H_6 and C_3H_8 reactions do not show significant difference from those reported by them, but the population in the low-N component is clearly seen in the CH_4 reaction.

TABLE 1: Ratio of the Vibrational Population between the $v'' = 0$ and 1 Levels

	$P_{v''=1}/P_{v''=0}$
bulk	
CH_4	1.1 ± 0.1
C_2H_6	0.79 ± 0.02
C_3H_8	0.43 ± 0.04
jet	
CH_4	1.1 ± 0.4

Vibrational Population. The LIF excitation spectra in the 1−1 region of OH $A\ ^2\Sigma^+ - X\ ^2\Pi$ transition were also measured for all reaction pairs. The recent studies reported a reaction mechanism that the rotational excitation of OH produced is accompanied with vibrational excitation; the low-N component with low vibrational excitation and the high-N component with vibrational excitation.[13,17] This is the case in this study; the fractions of $v'' = 1$ and high-N component become smaller in larger hydrocarbon. The vibrational distribution was obtained by summing up the population in each rotational level, and the results are listed in Table 1. The value in the CH_4 reaction is almost the same with the reported vibrational ratio of 1.0 in the 248 nm photolysis of the O_3/CH_4 system.[17] On the other

TABLE 2: Averaged Population Ratio, [Π(*A*′)]/[Π(*A*″)], of Two Λ Doublet States

	bulk condition		jet condition	
	$v'' = 0$	$v'' = 1$	$v'' = 0$	$v'' = 1$
CH_4	1.9 ± 0.30	1.3 ± 0.34	1.8 ± 0.30	1.5 ± 0.20
C_2H_6	1.8 ± 0.44	1.4 ± 0.30		
	1.6 ± 0.27[a]		1.7 ± 0.37[a]	–
C_3H_8	1.7 ± 0.31	1.4 ± 0.37		
	1.5 ± 0.25[b]		1.4 ± 0.30[b]	–

[a] For the sake of the comparison between the bulk and half-reactions, the values are obtained by averaging up to the same levels, $N'' = 14$, which is the highest measured level in the jet. [b] Averaged up to $N'' = 12$.

hand, the measured ratios, 0.79 and 0.43, in the C_2H_6 and C_3H_8 reactions are larger than those reported in the 248 nm O_3/C_2H_6 and C_3H_8 systems, ~0.4 and 0.2.

Population of Spin−Orbit States. The spin−orbit coupling in OH(X $^2\Pi$) produces the electronic fine structure, F_1 and F_2, which correspond to $^2\Pi_{3/2}$ and $^2\Pi_{1/2}$, respectively. The F_1 state was probed by the $P_1(N)$, $Q_1(N)$, and $R_1(N)$ transitions, and the F_2 state by the $P_2(N)$, $Q_2(N)$, and $R_2(N)$. The ratio between two states, F_1/F_2, was converted to $F_1N/F_2(N+1)$, where the factor, $N/(N+1)$, is the statistical weight. If OH is produced statistically in both states, the population is reflected with the degeneracy of rotation, $2J+1$. The measured ratio is very close to the statistical expectation for all rotational levels. The averages of the measured $F_1N/F_2(N+1)$ values are 1.1 ± 0.23, 1.2 ± 0.16, and 1.3 ± 0.24 in the $v'' = 0$ level and 1.0 ± 0.26, 1.0 ± 0.30, and 1.0 ± 0.32 in the $v'' = 1$ level for O(^{1}D) + CH_4, C_2H_6, and C_3H_8, respectively. It is clear that neither fine structure state is preferentially produced in both vibrational states in all reactant systems. This is consistent with that reported in the photolysis of O_3 before.[13,17]

Population of Λ Doublet States. In $\Lambda \neq 0$, coupling of rotational and electronic orbital angular momenta produces two Λ doublet states, which are labeled with Π(*A*′) and Π(*A*″) according to their symmetric properties. In the limit of high rotation, Π(*A*′) and Π(*A*″) correspond to the configurations in which the unpaired electron lobe lies on the plane of rotation and is perpendicular to the plane of rotation, respectively. Therefore, preference of the population to either state reflects the geometrical orientation of reaction intermediate leading to dissociation products. The Π(*A*′) population was determined with the *P* and *R* transitions and the Π(*A*″) with the *Q* transitions. The averaged ratios, [Π(*A*′)]/[Π(*A*″)], for all measured rotational states are summarized in Table 2. The ratio in all cases tends to increase as rotational quantum number increases in the same way reported previously. The preferential population to the Π(*A*′) state is clearly seen for the $v'' = 0$ level, while only slight preference is recognized for the $v'' = 1$ level. This supports the mechanism in which OH is produced by a prompt dissociation of the intermediate with keeping an orientated conformation formed by the insertion of O(^{1}D) atom to the hydrocarbon. All the measured values are 0.3−0.5 larger than those reported previously.[17] This indicates that the more defined plane conformation is achieved in the N_2O/193 nm system. As discussed later, it is considered that the average center-of-mass collision (translational) energy in the reaction system plays an important role in the rotational excitation of the high-*N* component.

The obtained ratio for $v'' = 0$ shows slight decrease with the size of hydrocarbon, which is considered to be due to the destroy of the oriented conformation during the dissociation resulting in the nonpreferential population of the Λ doublet and more production of the low-*N* component.

B. Reaction under Half-Collision Condition. LIF signals of reaction product OH were measured in the half-reactions. The LIF intensities in the O(^{1}D) + C_2H_6 and C_3H_8 reactions were much weaker than that in the CH_4 reaction. This is caused by predominant C−C bond fission yielding products other than OH in chemically activated alcohols formed in C_2H_6 and C_3H_8 reactions. It was reported that the total OH yields in the O(^{1}D) + C_2H_6 and C_3H_8 reactions were 0.033 and 0.056 relative to that in O(^{1}D) + CH_4 in the bulk reaction, respectively.[17]

Rotational distributions obtained by the same method mentioned above are shown in Figure 4a and b for $v'' = 0$ and 1 in the O(^{1}D) + CH_4 half-reactions, and in Figure 4c and d for $v'' = 0$ in the O(^{1}D) + C_2H_6 and C_3H_8 half-reactions, respectively. Highly rotational excitation of OH was observed in the CH_4 half-reaction, up to $N'' = 23$ for $v'' = 0$ and $N'' = 17$ for $v'' = 1$. On the other hand, the O(^{1}D) + C_2H_6 and C_3H_8 half-reactions give large population in low rotational levels comparing with the O(^{1}D) + CH_4 within the measured range up to $N'' = 13$. The distributions are apparently characterized by the bimodal (low- and high-*N* components) like those in the bulk reactions except for C_3H_8 which gives poor information due to low S/N ratio. The low-*N* components in $v'' = 0$ of the CH_4 half-reaction has large population than that in the corresponding bulk reaction. The distributions obtained in the jet seem to show similar feature with those observed under the bulk conditions.

In the O(^{1}D) + C_2H_6 and C_3H_8 reactions, the 1−1 band could not be detected in the jet experiments. Thus, vibrational population could be discussed only in the case of CH_4. The vibrational distribution was obtained by summing the population in each rotational level and its ratio between the $v'' = 0$ and 1 levels was estimated to be 1.1, which is same with that in the bulk reaction.

Obtained spin−orbit ratios are displayed in Figure 5 together with the expected statistical ratio for the reactions of O(^{1}D) with CH_4, C_2H_6, and C_3H_8 under the jet conditions. The results for $v'' = 0$ indicate nonstatistical behavior in low-*N* components for three hydrocarbons, where the low-lying electronic state, F_1, is preferentially populated. On the other hand, population ratio shows no preference to either state for $v'' = 1$ in the CH_4 half-reaction and the average value of $F_1N/F_2(N+1)$ is 1.1 ± 0.20.

The population ratios for Λ doublet states, [Π(*A*′)]/[Π(*A*″)], averaged for all measured rotational states are summarized in Table 2 together with those under the bulk conditions. All the measured values under the jet conditions are very close to those under the bulk conditions, that is, no specificity was recognized for Λ doublet states in the jet.

4. Discussion

A. Characterization of Two Components of Rotational Distribution. The measured rotational distributions in all reaction systems are evidently bimodal, and characterized with low- and high-*N* components. Rotational temperatures, T_{rot}, of the high-*N* components are directly derived from the rotational distributions in high internal energy regions assuming the Boltzmann distribution. The obtained temperatures for $v'' = 0$ and 1 are listed in Table 3. The rotational temperature of the high-*N* component for the O(^{1}D) half-reaction in the O_3/CH_4 system was reported to be ~5600 K, where O_3 was photolyzed at 266 nm.[20] Park and Wiesenfeld measured rotational distributions in the CH_4 and C_3H_8 bulk reactions but did not report the

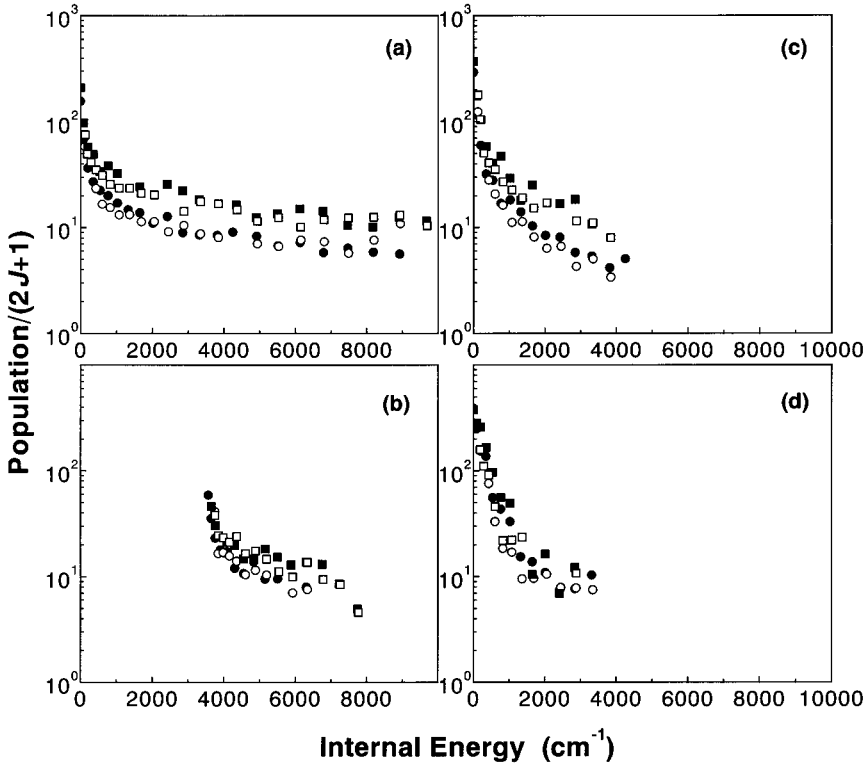

Figure 4. Nascent rotational distributions of product OH(X $^2\Pi$) in the half-reactions. (a) $v'' = 0$ level in the CH_4 reaction, (b) $v'' = 1$ level in the CH_4 reaction, (c) $v'' = 0$ level in the C_2H_6 reaction, and (d) $v'' = 0$ level in the C_3H_8 reaction. Symbols: ■, $F_1\Pi(A')$; □, $F_2\Pi(A')$; ●, $F_1\Pi(A'')$; and ○, $F_2\Pi(A'')$.

rotational temperature, where O(^{1}D) was generated by the 248 nm photolysis of O_3.[17] We estimated rotational temperatures of the high-*N* component to be ~7500 K using their data for the rotational energy between 4000 and 10 000 cm^{-1}. These temperatures are much lower than those obtained in this work. The average collision energy in these experiments is lower than that in this study. This indicates that the collision energy is efficiently reflected in the rotational excitation of the high-*N* component. It is noted that the change of rotational temperatures with the collision energy supports the short-lived insertion mechanism for the generation of the high-*N* component. The rotational temperatures obtained are almost same, ~13 000 K, in the three systems studied. This is another support for the short-lived insertion mechanism. The effects of collision energy and the change of substrate substantiate the mechanism that the excess energy is not randomized and is held in the C−O−H framework of intermediate ROH.

To obtain further characterization of two components, surprisal analysis is applied. Since the masses of reactants and products differ by only 1 amu in this light atom transfer, angular momentum constraints are relatively insignificant. The prior distribution requires only energy conservation and is calculated as the densities of energetically allowed rovibronic states of products at a given total energy using the method defined in ref 17, where all quantum states of products are assumed to have an equal probability.[17,29−31] Vibrational frequencies of the product alkyl radicals were estimated from those of references and parent molecules.[32−34]

The rotational surprisals, $I(f_r/f_v) = -\ln[P(v'',J'')/P^0(v'',J'')]$, are plotted as a function of the rotational fraction of the total available energy, g_R, and shown in Figure 6 for the CH_4 (a) bulk and (b) half-reactions, as typical cases. As seen in the figure, the enhanced population in the low-*N* component is apparently recognized in the half-reaction compared with the bulk reaction. The rotational surprisal in the O(^{1}D) + C_2H_6 bulk system is shown in Figure 7a and the surprisals for the high-*N* component was fitted by the linear approximation in the high fraction region. The rotational surprisal parameters, θ_R, were obtained from the slope, and are summarized in Table 4. Due to poor data points for the high-*N* components in the C_2H_6 and C_3H_8 half-reactions as seen in Figure 4, only CH_4 reaction was discussed for the half-reaction. The absolute values of θ_R are larger than the values reported,[13,17] which is thought to result mainly from the increase in collision energy. The large negative values indicate that product OH is highly excited in comparison with the expected statistical distribution in the high-*N* components. Furthermore, θ_R of the half-reaction is almost same as that of bulk reaction in the O(^{1}D) and CH_4 system.

As the high-*N* components were well characterized by linear rotational surprisals, the low-*N* components were abstracted by subtracting the high-*N* components characterized by linear surprisals from the measured distributions. The abstracted low-*N* component is shown in Figure 7b for the bulk reaction of C_2H_6 as an example. The low-*N* components were well characterized by Boltzmann plots in all reaction systems, and their T_{rot} are summarized in Table 3. As the rotational temperatures for the low-*N* components in the O_3/RH systems are not reported in refs 17 and 20, we estimated them to be ~1000 K by using the data in the references. The rotational temperatures measured in this study agree with the value estimated above. If reaction generating the low-*N* component is direct abstraction, increase of collision energy would rise the rotational temperature. On the other hand, if the OH formation follows the insertion of O(^{1}D) into C−H bond yielding a sufficiently long-lived collision complex enough to randomize the excess energy to various vibrational modes, the rotational temperature for low-*N* component is thought to be not sensitive to the collision energy. The obtained results support the latter mechanism.

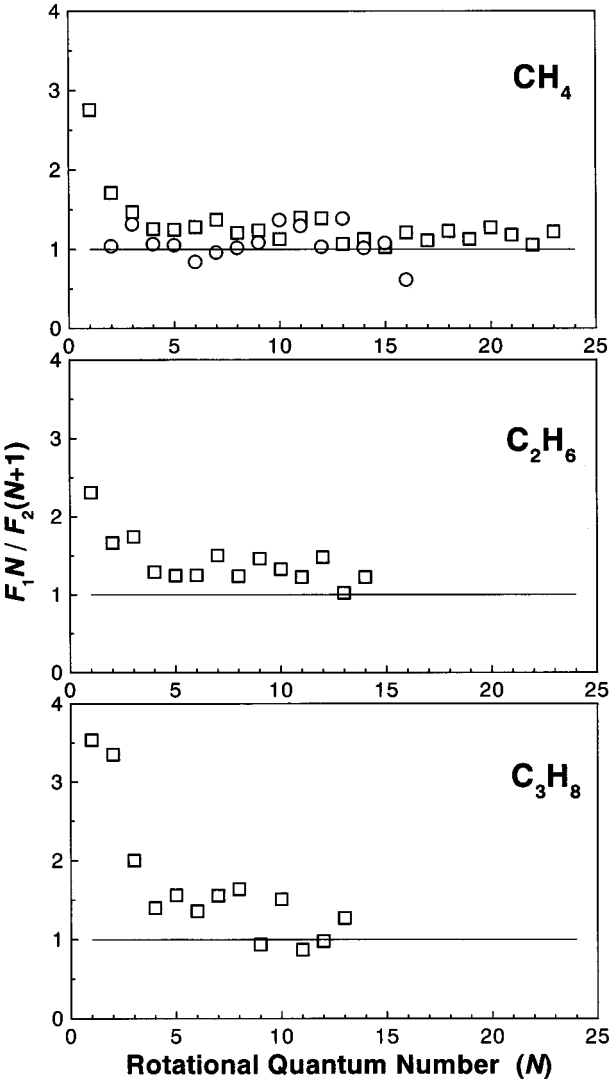

Figure 5. Population ratios of two spin−orbit states for the $v'' = 0$ (□) and 1 (○) levels of OH produced in the half-reactions of O(1D) with CH_4, C_2H_6, and C_3H_8. Solid lines show the statistical expectations.

TABLE 3: Measured Rotational Temperatures, T_{rot} (K)

	$v'' = 0$		$v'' = 1$	
reactant	low-N	high-N	low-N	high-N
bulk				
CH_4	960	12 600	1100	13 100
C_2H_6	1100	12 500	860	13 700
C_3H_8	820	12 900	1000	12 900
jet				
CH_4	1000	12 500	1100	13 100

As we can well characterize the low- and high-N components, the population ratios between them, P_{low-N}/P_{high-N}, were obtained as listed in Table 4. The ratio in the CH_4 half-reaction is larger than that in the corresponding bulk reaction, which indicates that the population in the low-N component is more pronounced in the CH_4 half-reaction.

B. Rotational Component of High-*N*. The energy partitioning in the reactions of O(1D) with hydrocarbons was discussed on the basis of the rotational distributions for high-N components in $v'' = 0$ of product OH. As discussed above, the rotational distributions for high-N components were efficiently enhanced with increase in the average collision energy, while those for low-N components show almost no change. The reactions studied in this paper have large available energy because of their large exothermicity.

Comes and Gericke studied energy partitioning in the O(1D) + $H_2{}^{18}O$ system.[35,36] The center-of-mass translational energy, $E_T(O,N_2)$, for the photodissociated O(1D) + N_2 is converted to the laboratory-frame translational energy as

$$E_{LAB}(O) = \frac{\mu_O}{m_O} E_T(O,N_2) + \frac{3}{2}\frac{m_O}{m_{N_2O}} R_g T \qquad (4)$$

where R_g is the gas constant, m_O and m_{N_2O} are the masses of O and N_2O, respectively, μ_O is the reduced mass in the O(1D) + N_2 system, and the second term arises from the thermal motion of N_2O. The center-of-mass collision energy in the reaction system of O(1D) with saturated hydrocarbon (RH) is

$$E_{col}(O, RH) = \mu_R \left(\frac{E_{LAB}(O)}{m_O} + \frac{3}{2}\frac{R_g T}{m_{RH}}\right)$$

$$= \mu_R \left[\frac{\mu_o}{m_O} E_T(O,N_2) + \frac{3}{2}\left(\frac{1}{m_{RH}} + \frac{1}{m_{N_2O}}\right) R_g T\right] \qquad (5)$$

where m_{RH} is the mass of RH, μ_R is the reduced mass in the O(1D) + RH system, and the term $3R_gT/2m_{RH}$ arises from the thermal motion of RH. The total available energy, E_{avail}, is determined by E_{col}(O,RH), the internal rovibrational energy of RH, $E_{int}(RH) = E_{vib}(RH) + E_{rot}(RH)$, and ΔH_r for reaction as

$$E_{avail} = E_{col}(O, RH) + E_{int}(RH) - \Delta H_r \qquad (6)$$

E_{int}(RH) was estimated at room temperature for bulk reaction. On the other hand, E_{int}(RH) and terms arising from the thermal motions were ignored for the half-reaction due to the cooling in the jet. The average rotational energy of product OH is obtained from

$$\langle E_{rot} \rangle = R_g T_{rot} \qquad (7)$$

where T_{rot} is the rotational temperature listed in Table 3. Energy disposal of O(1D) atom in the 193 nm photolysis of N_2O was reported,[28] in which O(1D) had the distribution in the translational energy due to the internal excitation of counter-fragment N_2. Accordingly, the average center-of-mass translational energy, $\langle E_T(O,N_2) \rangle$, was used, which was reported to be 114 kJ mol^{-1} in the photolysis of N_2O at 193 nm.[28] The calculated average collision energies, total available energies, and rotational energies are summarized in Table 5. The average center-of-mass translational energy, $\langle E_T(O,O_2) \rangle$,[39] in the 248 nm photolysis of O_3 is reported as 72.4 kJ mol^{-1} and, therefore, $\langle E_{avail} \rangle = 210$ kJ mol^{-1} in the O_3/CH_4 bulk reaction system of the 248 nm photolysis. From the reported rotational temperature for high-N component, ~7500 K,[17] the average rotational energy is estimated to be 62.4 kJ mol^{-1} and the fraction of the average rotational energy in the average total available energy is 29%. The corresponding fraction for the high-N component is obtained to be 47% in the N_2O/CH_4 bulk reaction system of the 193 nm photolysis, which is fairly large. Main difference between this and early experiments is the average collision energy, though the average total available energy does not significantly vary due to very large exothermicity of O(1D) reactions with saturated hydrocarbons. The rotational excitation for the high-N component (insertion process followed by the prompt dissociation) is enhanced with the increase of the collision energy. The average rotational energy in the N_2O/CH_4 bulk system of the 193 nm photolysis is 1.68 times of that in the 248 nm O_3/CH_4 system. This value is in good agreement with the ratio, 1.46, of the average collision energy in the 193 nm N_2O/CH_4 system

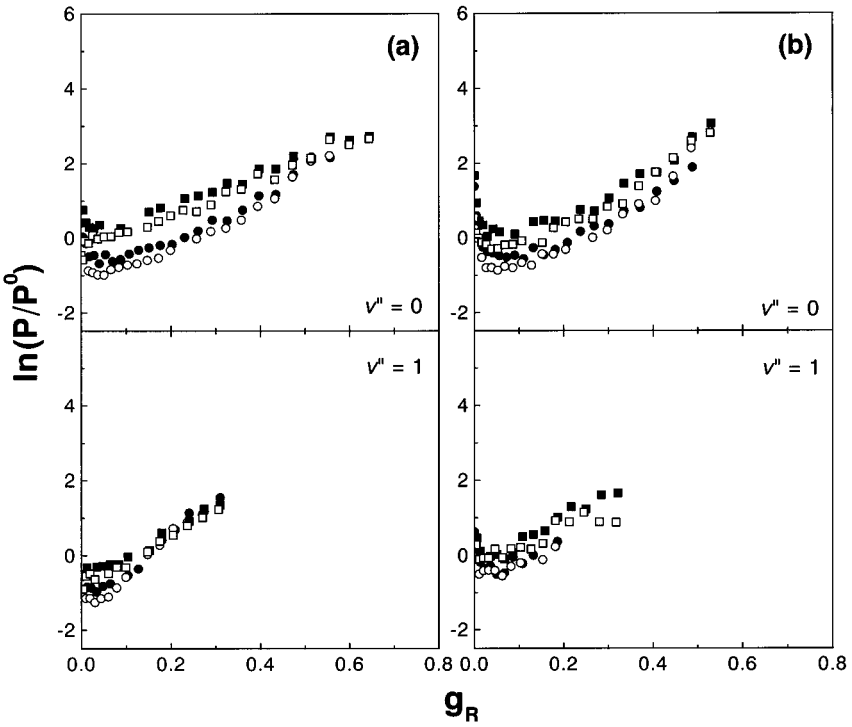

Figure 6. Rotational surprisal plots for $v'' = 0$ (upper) and 1 (lower) levels of nascent OH(X $^2\Pi$) produced in the CH_4 reactions. Conditions are: (a) bulk reactions; and (b) half-reactions. Symbols: ■, $F_1\Pi(A')$; □, $F_2\Pi(A')$; ●, $F_1\Pi(A'')$; and ○, $F_2\Pi(A'')$.

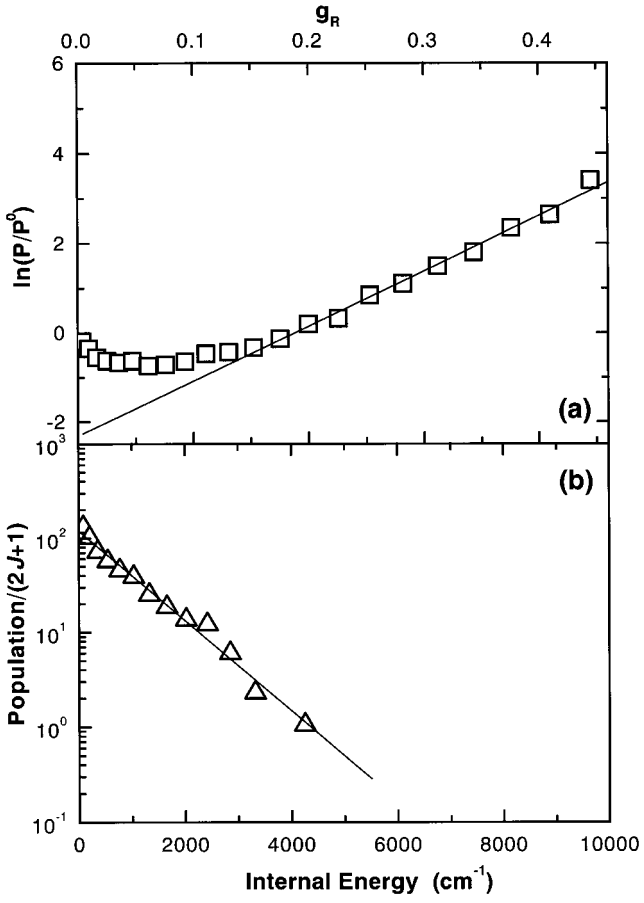

Figure 7. Nascent rotational population of OH produced in the C_2H_6 bulk reaction. (a) Rotational surprisal of Q_1 branch (□) and linear surprisal plot for high-N component (—). (b) Population of abstracted low-N component (△) and Boltzmann plot (—).

to that in the 248 nm O_3/CH_4 system. This kind of ratios was estimated in the C_3H_8 bulk and CH_4 half-reactions as listed in Table 5, together with the reported values.[17,20] The ratios of the average rotational energies also agree well with those of the average collision energies. The potential surface for the reaction of $O(^1D)$ with CH_4 calculated by Arai et al. has a very low potential barrier of 8.8 kJ mol^{-1} in the entrance region of the reaction.[22] Taking account of the barrier, the excess energy in the N_2O/CH_4 bulk system of the 193 nm photolysis is calculated to be 1.68 times of that in the 248 nm O_3/CH_4 system, which coincides very well with the ratio of the average rotational energy for high-N component. The results in other reaction systems also show good coincidence (Table 5). It can be considered that the average center-of-mass collision energy (translational energy) in the reaction system plays an important role in the rotational excitation for the high-N component, which is produced by the insertion followed by the prompt dissociation of the reaction intermediate. In other words, the initial memory included in the reaction system is well retained beyond the activation barrier. This means that alkyl groups behave like a spectator in the reaction and, therefore, the vibrational excitation of product alkyl radicals is thought to be not so high. This is consistent with the observation of the noninverted ν_2 (umbrella mode) excitation of the product CH_3 formed in the $O(^1D) + CH_4$ reaction.[15,16]

TABLE 4: Rotational Surprisal Parameter, θ_R, and the Ratio, P_{low-N}/P_{high-N}, of Populational Fraction between Low- and High-N Components

	$-\theta_R$		P_{low-N}/P_{high-N}	
	$v'' = 0$	$v'' = 1$	$v'' = 0$	$v'' = 1$
bulk				
CH_4	7.0	6.9	0.19	0.05
C_2H_6	12.3	13.0	0.41	0.06
C_3H_8	17.1	16.5	2.3	0.06
jet				
CH_4	6.8	6.9	0.32	0.07

Arai et al. calculated the potential energy surface in the $O(^1D) + CH_4$ reaction in restricted C_s symmetry by the ab initio multireference single and double configuration interaction

TABLE 5: Summary of the Rotational Energetics (kJ mol^{-1})

			N_2O/RH system				O_3/RH system		
			bulk (193 nm)			jet (193 nm)	bulk (248 nm)[a]		jet (266 nm)[b]
			CH_4	C_2H_6	C_3H_8	CH_4	CH_4	C_3H_8	CH_4
ΔH_r			180	208	200[c]	182	180	200[c]	182
$\langle E_{col}(O,RH)\rangle$			38.9	49.5	55.2	36.3	26.7	37.3	18.7[d]
$\langle E_{avail}\rangle$			222	263	263	218	210	246	201
$\langle E_{rot}\rangle$	$v''=0$	low-N	7.9	9.1	6.8	8.4	8.3	8.3	8.3
		high-N	105	104	107	104	62.4	62.4	46.6
	$v''=1$	low-N	8.8	7.1	8.6	8.9			
		high-N	110	114	107	109			
fraction of $\langle E_{rot}\rangle$[e]	$v''=0$	low-N	3.5	3.5	2.6	3.8	3.9	3.4	4.1
		high-N	47	40	41	48	29	25	23
ratio of $\langle E_{col}\rangle$[f]			1.46		1.48	1.36	1.0	1.0	0.70
ratio of $\langle E_{col}\rangle$[f,g]			1.68		1.63	1.54	1.0	1.0	0.56
ratio of $\langle E_{rot}\rangle$[h]	$v''=0$	high-N	1.68		1.72	1.67	1.0	1.0	0.75

[a] Taken from ref 17. [b] Taken from ref 20. [c] $\Delta H_r = -200$ kJ mol^{-1} for the production of n-C_3H_7 was used in the C_3H_8 reaction because it was demonstrated from a study of O(^{1}D) + $CH_3CD_2CH_3$ bulk reaction that product OH was dominantly produced from primary position of C_3H_8 than secondary position.[37] [d] $\langle E_{col}(O, RH)\rangle$ was calculated by using reported value of $\langle E_T(O,O_2)\rangle$, 56.1 kJ mol^{-1} in the O_3/266 nm system.[38] [e] Calculated as the fraction of $\langle E_{avail}\rangle$ (%). [f] Calculated as the ratio to $\langle E_{col}(O, RH)\rangle$ in the corresponding RH bulk reaction in the O_3/248 nm system. [g] Ratio was obtained by considering the potential barrier reported in ref 22. The potential barrier in the C_3H_8 reaction was regarded as the same in the CH_4. [h] Calculated as the ratio to $\langle E_{rot}\rangle$ in the corresponding RH bulk reaction in the O_3/248 nm system.

method.[22] The potential indicates that the minimum energy path for the reaction is the collinear approach of O(^{1}D) atom to the H end of the C−H bond. They suggested existence of a saddle point in the entrance region of the reaction surface in the course of the minimum energy path, during which the CH_4 moiety almost keeps the stable CH_4 structure. After the saddle point, O(^{1}D) moves off from the C−H axis and the structure approaches to that of the stable CH_3OH very rapidly (insertion process). In this process, the angle of C−H−O skeleton changes from 180° to about 50° and then OH removes from CH_3 keeping almost the same C−H−O angle. Therefore, in the course of the reaction, a relatively large amount of energy may be used to make torque of the OH moiety until the chemically activated intermediate (methanol) is formed. If the collision energy is enlarged on such a potential surface, the reaction process forming the intermediate proceeds rapidly and the rotation of the OH moiety is enhanced; the increase in the collision energy is reflected in rotational excitation of OH as seen before.

It is also noted that the averaged population ratios of Λ doublet states studied here are a little larger than those in the O_3/RH system reported previously.[17] This is a reasonable result because the plane conformation of C−O−H of the intermediate is retained during the dissociation, as the torque of the rotation of the OH moiety on the attractive entrance potential surface is more enhanced with enlarged collision energy.

C. Half-Collision Reaction. Studies of half-reactions photoinitiated in a vdW complex frequently bring us peculiar results in comparison with those obtained in the corresponding bulk reactions. It is reported that a third body effect is not negligible in some half-reactions;[40,41] in the photoinitiated half-reaction, the counterpart of photolyzed molecule exists near the reactant and, therefore, affects the reaction. However, van Zee et al. reported that there was no third body effect in the O_3/CH_4 half-reaction and explained that the large exothermicity of the O(^{1}D) + CH_4 reaction overcame third body effect.[20] The half-reactions of O(^{1}D) with saturated hydrocarbons studied here do not give significantly different results for E_{rot} (or T_{rot}), the vibrational population, or the population ratio of Λ doublet states from those obtained in the corresponding bulk reactions, and no third body effect is recognized. As mentioned before, the average collision energy is directly reflected in the average rotational energy in similar way under the bulk and jet conditions. This is more evidence of the absence of the third body effect.

However, two obvious differences from the bulk reactions appeared in low-N component of the half-reactions, that is, the more pronounced population especially in the CH_4 reaction and the apparent propensities of lower lying spin−orbit (F_1) states for all hydrocarbons studied here. It should be noted that the low-N component is generated by the dissociation of a long-lived intermediate produced by the insertion reaction of O(^{1}D) to a C−H bond. The entrance channel of O(^{1}D) + saturated hydrocarbon correlates equivalently to two spin−orbit states, F_1 and F_2, of the product OH and does not directly bring about the preference to the low-lying F_1 ($^2\Pi_{3/2}$) state. Figure 8 shows a schematic correlation diagram for the O + hydrocarbon reaction. There is a crossing around the entrance region.[42] If the crossing occurs and the total electronic angular momentum ($J = 2$) of O(^{1}D) is conserved during the crossing, O(^{1}D) correlates to the O(^{3}P$_2$) + hydrocarbon surface as the crossing exists in the entrance region. It is known that the mixing between the singlet and triplet states is very efficient through the crossing point when a long-lived collision complex is formed.[43,44] The O(^{3}P$_2$) + hydrocarbon surface only correlates to the F_1 state of OH (see Figure 8). The propensity for the F_1 state is, therefore, caused by the crossing. This explanation is consistent with the reaction mechanism described before and experimental results: the propensity for the F_1 state was observed only in the low-N component, which was generated via the long-lived intermediate.

The propensities for the F_1 state in the O(^{1}D) reactions were also reported on the CH_4 clusters and propane reactions in the crossed molecular beam by Naaman and co-workers.[18] They answered to the question why the electronic angular momentum was conserved during the curve crossing from the singlet to the triplet surface. The total angular momentum in the reactant system has two components; the orbital angular momentum due to the impact parameter and the initial angular momentum of the reactants. In the jet experiment, the angular momentum associated with the nuclear rotation is small due to the cooling of reactants. If the collisions of the reactants occur with the small impact parameter, the electronic angular momentum is the only angular momentum in the system. If angular momen-

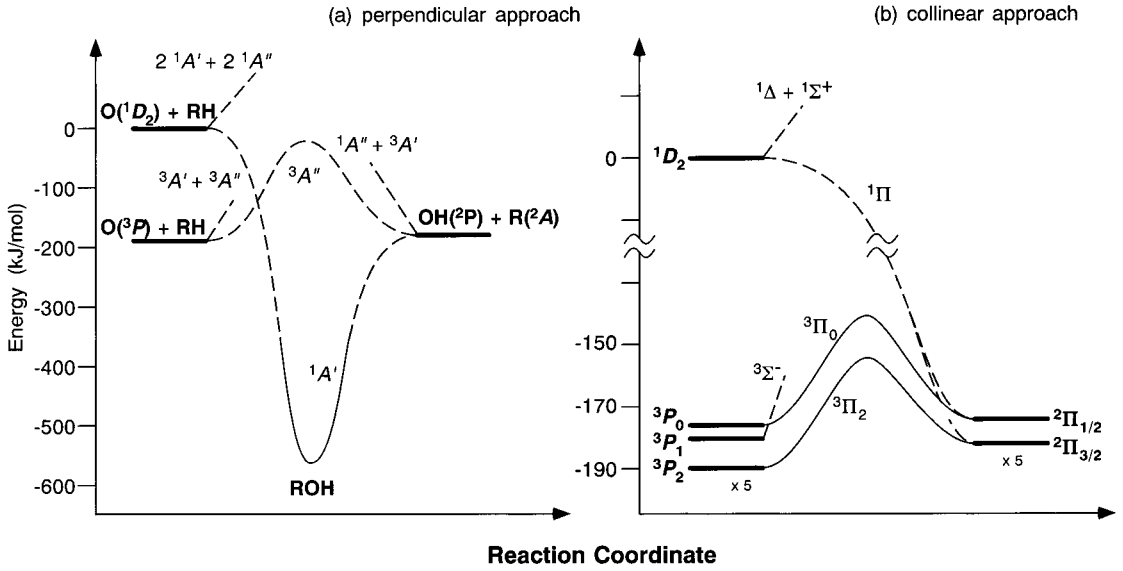

Figure 8. Schematic correlation diagrams for the reaction of O atom with hydrocarbon taken from refs 13 and 23. (a) O atom is assumed to approach perpendicularly to the C−H bond of hydrocarbon. (b) Collinear approach. Energies are shown for the CH_4 reaction, and the splittings in the $O(^3P_j)$ and the spin−orbit states are shown with a scale expansion of 5.

tum caused by the nuclear motion during the cause of reaction is included in the total angular momentum, the electronic angular momentum is not conserved and, therefore, no propensity is observed. The experimental results that the propensities are observed only in the low-*N* components of the $v'' = 0$ level and monotonically decrease as the rotational quantum number increases are consistent with the conservation of the electronic angular momentum during the reaction.

Although no propensity of spin−orbit states was recognized in the CH_4 crossed molecular beam[18] and the O_3/CH_4 half-reactions,[20] the propensities were apparently observed even in the N_2O/CH_4 half-reaction as well as the C_3H_8 crossed beam[18] and the N_2O/ C_2H_6 and C_3H_8 half-reactions. A question arises why the propensity appears in the C_3H_8 but not in the CH_4 reactions in the crossed beam experiments. The lifetime of the insertion reaction intermediates gives one of the answers for this question.[18] Another possibility is, however, explored in the impact parameter. The contribution of the reaction with a small impact parameter would be more emphasized in the C_3H_8 reaction than in the CH_4 reaction due to the larger spatial extent of hydrogen atoms. In the half-reactions, the N_2O/CH_4 vdW complex gives propensity but O_3/CH_4 does not. The N_2O/CH_4 vdW complex may be considered to have a favorable conformation to promote the reaction with a small impact parameter than O_3/CH_4 does. The study of the structures of N_2O and O_3/hydrocarbon vdW complexes, on which we have no information, would bring about further understanding about the reaction mechanism.

5. Summary

The bulk and half-reactions of $O(^1D)$ with saturated hydrocarbons, CH_4, C_2H_6, and C_3H_8, are studied, where $O(^1D)$ is produced by the ArF excimer laser photolysis of N_2O. In the latter case, the reaction was initiated from the vdW complex of reactant precursor, $N_2O{\cdot}RH$. The nascent population distribution of reaction product $OH(X\ ^2\Pi,\ v'' = 0, 1)$ was measured by means of the LIF technique.

The rotational distributions are bimodal, which are denoted with the low- and high-*N* components. In comparison with the reported results obtained in the O_3 photolysis system, the obvious difference in the average rotational energy for the high-*N* components is recognized, while the average rotational energy for the low-*N* components does not show apparent difference. The reaction mechanism and dynamics producing characteristically bimodal components are discussed by comparing the populations of OH obtained under different reaction conditions.

The rotational energy of the low-*N* component does not depend on experimental conditions; average collision energy and the bulk and half-reactions. The rotational temperature is low, ca. 1000 K. The low-*N* component is verified to be generated by the dissociation of a long-lived intermediate produced by the insertion reaction, in which the excess energy is randomized before dissociation.

On the other hand, the rotational energy of the high-*N* component is changed with the average collision energy and the temperature is very high, ca. 13 000 K. The high-*N* component is confirmed to be formed from a short-lived intermediate produced by the insertion reaction. The increase of the collision energy is reflected in the increase of the rotational energy. This is due to that the excess energy is fundamentally distributed among the local framework of C−O−H of the intermediate, which is also supported by larger values of the population ratios for Λ doublet states in this study than those obtained in the O_3 photolysis system.

Spin−orbit populations in all $v'' = 0$ levels under the half-collision conditions indicate pronounced populations for low-lying F_1 state in low-*N* components, while those under the bulk conditions are statistical. It is thought that the reaction of all saturated hydrocarbons studied here occurs via a crossing from a singlet to a triplet surface keeping the angular momentum conservation.

Acknowledgment. The authors thank Professor I. Hanazaki and Dr. N. Tanaka for their support of the Joint Studies Program (1995−1996) of the Institute for Molecular Science. The present work is partly supported by a Grant-in-Aid on Priority-Area-Research on "Photoreaction Dynamics" from the Ministry of Education, Science, Sports, and Culture of Japan (No. 06239103).

References and Notes

(1) Donovan, R. J.; Husain, D. *Chem. Rev.* **1970**, *70*, 489.
(2) Lin, M. C. *Adv. Chem. Phys.* **1980**, *42*, 113.

(3) Wiesenfeld, J. R. *Acc. Chem. Res.* **1982**, *15*, 110.
(4) Warneck, P. *Chemistry of the Natural Atmosphere*; Academic Press: San Diego, CA, 1988.
(5) Crosley, D. R. *J. Atmos. Sci.* **1995**, *52*, 3299.
(6) Basco, N.; Norrish, R. G. W. *Can. J. Chem.* **1960**, *38*, 1769.
(7) (a) Yamazaki, H.; Cvetanović, R. J. *J. Chem. Phys.* **1964**, *41*, 3703. (b) Paraskevopoulos, G.; Cvetanović, R. J. *J. Chem. Phys.* **1969**, *50*, 590. (c) Paraskevopoulos, G.; Cvetanović, R. J. *J. Chem. Phys.* **1970**, *52*, 5821. (d) Michaud, P.; Cvetanovic′, R. J. *J. Chem. Phys.* **1972**, 76, 1375.
(8) (a) DeMore, W. B.; Raper, O. F. *J. Chem. Phys.* **1967**, *46*, 2500. (b) Lin, C.-L.; DeMore, W. B. *J. Phys. Chem.* **1973**, *77*, 863.
(9) (a) Greenberg, R. I.; Heicklen, J. *Int. J. Chem. Kinet.* **1972**, *4*, 417. (b) Jayanty, R. K. M.; Simonaitis, R.; Heicklen, J. *Int. J. Chem. Kinet.* **1976**, *8*, 107.
(10) Casavecchia, P.; Buss, R. J.; Sibener, S. J.; Lee, Y. T. *J. Chem. Phys.* **1980**, *73*, 6351.
(11) Aker, P. M.; O'Brien, J. J. A.; Sloan, J. J. *J. Chem. Phys.* **1986**, *84*, 745.
(12) Cheskis, S. G.; Iogansen, A. A.; Kulakov, P. V.; Razuvaev, I. Y.; Sarkisov, O. M.; Titov, A. A. *Chem. Phys. Lett.* **1989**, *155*, 37.
(13) Luntz, A. C. *J. Chem. Phys.* **1980**, *73*, 1143.
(14) Satyapal, S.; Park, J.; Bersohn, R.; Katz, B. *J. Chem. Phys.* **1989**, *91*, 6873.
(15) Suzuki, T.; Hirota, E. *J. Chem. Phys.* **1993**, *98*, 2387.
(16) Schlütter, J.; Schott, R.; Kleinermanns, K. *Chem. Phys. Lett.* **1993**, *213*, 262.
(17) Park, C. R.; Wiesenfeld, J. R. *J. Chem. Phys.* **1991**, *95*, 8166.
(18) (a) Rudich, Y.; Hurwitz, Y.; Frost, G. J.; Vaida, V.; Naaman, R. *J. Chem. Phys.* **1993**, *99*, 4500. (b) Hurwitz, Y.; Rudich, Y.; Naaman, R. *Chem. Phys. Lett.* **1993**, *215*, 674. (c) Hurwitz, Y.; Rudich, Y.; Naaman, R. *Isr. J. Chem.* **1994**, *34*, 59.
(19) (a) Brouard, M.; Duxon, S. P.; Enriquez, P. A.; Simons, J. P. *J. Chem. Soc., Faraday Trans.* **1993**, *89*, 1435. (b) Brouard, M.; Duxon, S. P.; Simons, J. P. *Isr. J. Chem.* **1994**, *34*, 67.
(20) (a) van Zee, R. D.; Stephenson, J. C.; Casassa, M. P. *Chem. Phys. Lett.* **1994**, *223*, 167. (b) van Zee, R. D.; Stephenson, J. C. *J. Chem. Phys.* **1995**, *102*, 6946.
(21) Nakajima, M.; Tsuda, M.; Oikawa, S. *Chem. Pharm. Bull.* **1987**, *35*, 941.
(22) Arai, H.; Kato, S.; Koda, S. *J. Phys. Chem.* **1994**, *98*, 12.
(23) Andresen, P.; Luntz, A. C. *J. Chem. Phys.* **1980**, *72*, 5842.
(24) (a) McNesby, J. R.; Okabe, H. *Adv. Photochem.* **1964**, *3*, 157. (b) Okabe, H. *Photochemistry of Small Molecules*; Wiley: New York, 1978.
(25) Dieke, G. H.; Crosswhite, H. M. *J. Quant. Spectrosc. Radiat. Transfer* **1962**, *2*, 97.
(26) Chidsey, I. L.; Crosley, D. R. *J. Quant. Spectrosc. Radiat. Transfer* **1980**, *23*, 187.
(27) Brzozowski, J.; Erman, P.; Lyyra, M. *Phys. Scr.* **1978**, *17*, 507.
(28) Springsteen, L. L.; Satyapal, S.; Matsumi, Y.; Dobeck, L. M.; Houston, P. L. *J. Phys. Chem.* **1993**, *97*, 7239.
(29) Bernstein, R. B. *Atom−Molecule Collision Theory: A Guide for the Experimentalist*; Plenum: New York, 1979.
(30) Bogan, D. J.; Setser, D. W. *J. Chem. Phys.* **1976**, *64*, 586.
(31) Robinson, P. J.; Holbrook, K. A. *Unimolecular Reactions*; Wiley-Interscience: New York, 1972.
(32) Jacox, M. E. *J. Phys. Chem. Ref. Data* **1994**, Monograph No. 3.
(33) Flurry, R. L., Jr. *J. Mol. Spectrosc.* **1975**, *56*, 88.
(34) The Chemical Society of Japan. *Kagaku Benran (Chemical Tables)*, 4th ed.; Maruzen: Tokyo, 1993.
(35) Comes, F. J.; Gericke, K.-H. *J. Chem. Phys.* **1981**, *75*, 2853.
(36) Tanaka, N.; Takayanagi, M.; Hanazaki, I. *Chem. Phys. Lett.* **1996**, *254*, 40.
(37) Wada, S.; Obi, K. Unpublished.
(38) Sparks, R. K.; Carlson, L. R.; Shobatake, K.; Kowalczyk, M. L.; Lee, Y. T. *J. Chem. Phys.* **1980**, *72*, 1401.
(39) Thelen, M.-A.; Gejo, T.; Harrison, J. A.; Huber, J. R. *J. Chem. Phys.* **1995**, *103*, 7946.
(40) Shin, S. K.; Chen, Y.; Nickolaisen, S.; Sharpe, S. W.; Beaudet, R. A.; Witting, C. *Adv. Photochem.* **1991**, *16*, 249.
(41) Takayanagi, M.; Hanazaki, I. *Chem. Rev.* **1991**, *91*, 1193.
(42) This is assumed from the analogous reaction of O(^{1}D) + H_2, in which it was calculated that the crossing existed in the entrance region in nonlinear conformation (Howard, R. E.; McLean, A. D.; Lester, W. A., Jr. *J. Chem. Phys.* **1979**, *71*, 2412).
(43) Tully, J. C. *J. Chem. Phys.* **1974**, *61*, 61.
(44) Zahr, G. E.; Preston, R. K.; Miller, W. H. *J. Chem. Phys.* **1975**, *62*, 1127.